PCCP

PAPER

View Article Online
View Journal | View Issue

Cite this: *Phys. Chem. Chem. Phys.*, 2016, **18**, 31107

Hot exciton cooling and multiple exciton generation in PbSe quantum dots†

Manoj Kumar,[a] Stefano Vezzoli,[b] Zilong Wang,[a] Varun Chaudhary,[cd] Raju V. Ramanujan,[d] Gagik G. Gurzadyan,[ae] Annalisa Bruno*[f] and Cesare Soci*[ab]

Received 1st June 2016,
Accepted 19th October 2016

DOI: 10.1039/c6cp03790a

www.rsc.org/pccp

Multiple exciton generation (MEG) is a promising process to improve the power conversion efficiency of solar cells. PbSe quantum dots (QDs) have shown reasonably high MEG quantum yield (QY), although the photon energy threshold for this process is still under debate. One of the reasons for this inconsistency is the complicated competition of MEG and hot exciton cooling, especially at higher excited states. Here, we investigate MEG QY and the origin of the photon energy threshold for MEG in PbSe QDs of three different sizes by studying the transient absorption (TA) spectra, both at the band gap (near infrared, NIR) and far from the band gap energy (visible range). The comparison of visible TA spectra and dynamics for different pump wavelengths, below, around and above the MEG threshold, provides evidence of the role of the Σ transition in slowing down the exciton cooling process that can help MEG to take over the phonon relaxation process. The universality of this behavior is confirmed by studying QDs of three different sizes. Moreover, our results suggest that MEG QY can be determined by pump–probe experiments probed above the band gap.

1. Introduction

The power conversion efficiency of a single semiconductor junction solar cell (SC) can be, theoretically, as high as 33%.[1] At the moment in a conventional SC, most of the absorbed energy is dissipated as heat. Indeed, in a semiconductor, when the energy ($h\nu$) of an absorbed photon is higher than the energy band gap (E_g), hot carriers are generated. Hot carriers quickly cool down to the band edge and release their excess energy to phonons (thermal dissipation). In bulk semiconductors the distribution of energy levels is continuous, so the coupling with phonons is very efficient and consequently the excess energy of hot carriers is quickly dissipated.[2] The process of cooling down of hot carriers is then a major energy loss channel in photovoltaic devices.[2,3] In contrast, in quantum confined nanostructures, the energy levels are discrete, and the energy difference between two consequent energy levels can be much higher than the phonon energy. Therefore, when the energy of the absorbed photon is at least twice the energy band gap, a significant portion of the excess energy of hot excitons can be transferred to electrons/holes in the valence band, the hot exciton cooling process through phonons is reduced,[4,5] and one or more new excitons can be created. This process is known as multiple exciton generation (MEG)[6–15] and, in principle, it allows a great improvement of the SC power conversion efficiency.[6,16–18]

Typical MEG quantum yield (QY) values in quantum dots (QDs) are between 1 and 3 with photon energy excitation 2 to 5 times the band gap of the QDs.[2,19–22] However, there is still an on-going debate about the parameters influencing the MEG QY,[23] since other works have shown very low MEG QY even at much higher photon energy.[24–27] One of the reasons for this inconsistency may be the complicated competition of MEG and the hot exciton de-excitation process, especially at higher excited states. In particular, one of the open questions is how the threshold energy for MEG is influenced by other physical phenomena. In principle, the threshold should be two times E_g, but it turns out to be higher since phonon relaxation rates are normally larger than the MEG rate. Recently, it has been pointed out that the electronic transition, corresponding to the Σ point in the Brillouin zone‡[28] called the Σ transition, could

[a] *Division of Physics and Applied Physics, School of Physical and Mathematical Sciences, Nanyang Technological University, 21 Nanyang Link, Singapore, 637371, Singapore. E-mail: csoci@ntu.edu.sg*
[b] *Centre for Disruptive Photonic Technologies, School of Physical and Mathematical Sciences, Nanyang Technological University, 21 Nanyang Link, Singapore, 637371, Singapore*
[c] *Interdisciplinary Graduate School (IGS), Nanyang Technological University, 50 Nanyang Avenue, Singapore, 639798, Singapore*
[d] *School of Materials Science and Engineering, Nanyang Technological University, 50 Nanyang Avenue, Singapore 639798, Singapore*
[e] *Institute of Artificial Photosynthesis, State Key Laboratory of Fine Chemical, Dalian University of Technology, Dalian, 116024, China*
[f] *Energy Research Institute @ NTU (ERI@N), Research Techno Plaza, X-Frontier Block, 50 Nanyang Drive, Singapore, 637553, Singapore. E-mail: annalisa@ntu.edu.sg*

† Electronic supplementary information (ESI) available. See DOI: 10.1039/c6cp03790a

‡ Σ point is defined as the second extremum (maxima of the valence band and minima of the conduction band) in the Brillouin zone.

play an important role in determining the threshold for MEG.[4] It has been suggested that the hot exciton cooling process could slow down around this level, allowing the MEG process to overcome the cooling rate of phonons.[4] This would imply that MEG has an energy threshold strictly higher than the Σ transition.[4,8,10,29] The Σ transition is observed in both bulk and QDs and its position shifts towards higher energy with the decreasing size of QDs.[28]

PbSe QDs are widely explored as materials for SC, infrared (IR) lasers, diodes, and IR-detector applications. PbSe QDs, due to their large Bohr radius (46 nm), show large quantum confinement effects[30] exhibiting narrow emission ranging from near infrared (NIR) to mid-infrared (IR).[31] Most of the previous spectroscopic studies on PbSe QDs have been performed near the band edge,[2,8,32–36] which is at the bottom of the cooling cascade process through the higher energy states, where 1P–1S transition is the last step of the cooling cascade, and thus clear information of the higher energy levels cannot be extracted from the rise time of the photobleaching signal. Therefore, in these studies only the cooling process from 1P to 1S, is assessed by probing states in the NIR region, close to the QD band gap. The competition between hot exciton cooling and MEG cannot be observed and quantified in the band edge measurements.

In this paper, we determine MEG threshold energy and MEG QY for PbSe QDs of three different sizes through NIR transient absorption (TA) spectroscopy. We also investigated the origin of the threshold energy for MEG in PbSe QDs through the analysis of TA spectra, in the visible region close to the Σ transition, at different pumping energies. We show evidence of a reduction of the hot exciton cooling down *via* phonon relaxation around the Σ point, where the MEG starts taking over the phonon relaxation process. Moreover, by comparing the TA dynamics at and above the PbSe QD band gap, we also infer that the MEG QY could be measured directly from the visible TA spectra (above the band gap), which are generally easier to measure compared to the NIR TA spectra.

2. Methodology

2.1 Materials, sample preparation and characterization

Three different types of PbSe QDs having absorption peaks at 1100 nm (QD_1), 1200 nm (QD_2) and 1300 nm (QD_3), respectively, have been bought from NN Crystal US Corporation suspended in hexane with an initial concentration of 10 mg ml^{-1}. They were diluted around 10 times to avoid the absorption of most of the pumping photons by the front surface of the sample and then filled in quartz cuvettes of 1 mm optical path length for all the optical measurements.

The absorption spectra of PbSe QDs were measured on a Perkin Elmer Lambda 750 UV/Vis/NIR spectrophotometer with 1 nm wavelength resolution. Photoluminescence (PL) spectra were measured using a FluoroLog-3 spectrophotometer with a wavelength resolution of 0.5 nm using a nitrogen cooled InGaAs detector (Electro-Optical Systems). All measurements were performed at room temperature.

The particle size and morphology of PbSe QDs were determined by using a JEOL JEM-2010/UHR transmission electron microscope (TEM) at an operating voltage of 200 kV. The hexane suspended PbSe QDs were dropped on a holey carbon-coated copper grid and allowed to dry in a vacuum for one night before being measured. Averaged QD sizes were determined from TEM images using the Image J software. From the images individual particles sizes were extrapolated and a histogram distribution was generated. The average QD size was then calculated by Gaussian fitting of the histograms.

2.2 Transient absorption (TA) measurements

TA setup schemes for visible and NIR measurements are shown in Fig. S1(a) and (b) in the ESI.† In both configurations, the fundamental (800 nm) light beam of a Ti:sapphire femtosecond laser (repetition rate 1 KHz, pulse length around 100 fs and 2 W power), the second (SH, 400 nm) and the third (TH, 267 nm) harmonics were used as pump beams. The SH was generated using a type-1 BBO crystal (phase matching angle 29.2°), while the TH was formed by the sum frequency generation of 400 nm and 800 nm in a type-2 BBO crystal (phase matching angle 55.5°). The pump laser power was tuned by a neutral density (ND) filter and kept low throughout the measurements to minimize the nonlinear multiple-photon absorption by QDs.

The white light continuum (WLC_{VIS}) used as probe light for visible TA experiments shown in Fig. S1(a) (ESI†) was generated by focusing the 800 nm beam onto a 2 mm thick sapphire plate. WLC_{VIS} was focused on the sample and the spectra were measured using a CCD camera (Entwicklungsburo Stresing) with the detection range from 200 nm to 950 nm. The white light continuum (WLC_{NIR}) probe light for NIR TA measurements was generated by focusing 1620 nm laser light from an optical parametric amplifier (OPA, Palitra-FS Quantronix) onto a 4 mm thick yttrium aluminium garnet (YAG) crystal.[37] The residue of 1620 nm from the WLC_{NIR} was filtered by a short-pass mirror (Thorlabs DMSP1500). WLC_{NIR} was focused on the sample and the signal was detected by using a NIR photodiode array (PDA) (Entwicklungsburo Stresing) in the range from 950 nm to 1450 nm. The samples were always shaken by a motorized stage during measurements to minimize the photochemical decomposition.

3. Results and discussion

3.1 PbSe QDs

The TEM images of PbSe QD_1, QD_2 and QD_3 are shown in Fig. 1(a)–(c), respectively. All QDs have a spherical shape and their average diameters, estimated from the TEM images are 3.6 ± 0.3 nm, 3.8 ± 0.5 nm and 4.3 ± 0.5 nm for QD_1, QD_2 and QD_3, respectively. QD size distributions are shown in Fig. S2 in the ESI.† In Fig. 1(d)–(f) absorption (left axis) and PL (right axis) spectra of QD_1, QD_2 and QD_3 are shown, with first excitonic absorption peaks at ~1100 nm, ~1200 nm and ~1300 nm and PL peaks at ~1170 nm, ~1260 nm and ~1350 nm, respectively. The well-defined first excitonic peaks in the absorption spectra of all QD samples correspond to the band gap energy (E_g) value. As expected, we consistently observe a red shift in the measured first excitonic absorption as well as PL peaks coinciding well with the increasing size of QDs obtained from TEM images.

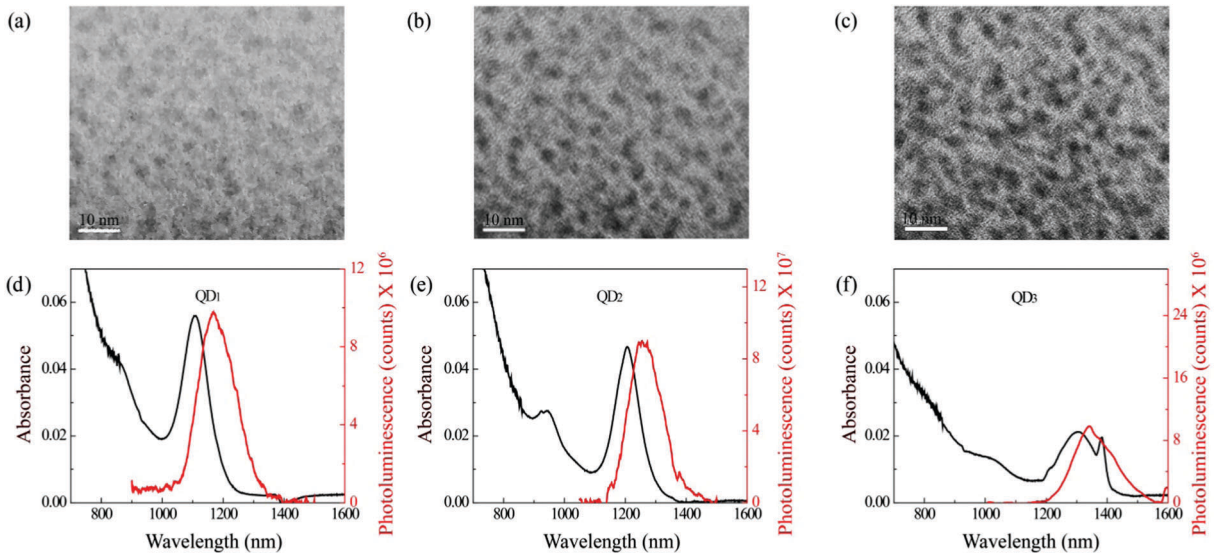

Fig. 1 TEM images of (a) QD_1, (b) QD_2 and (c) QD_3. Steady state absorption (left axis) and photoluminescence spectra (right axis), at 800 nm excitation for (d) QD_1, (e) QD_2 and (f) QD_3.

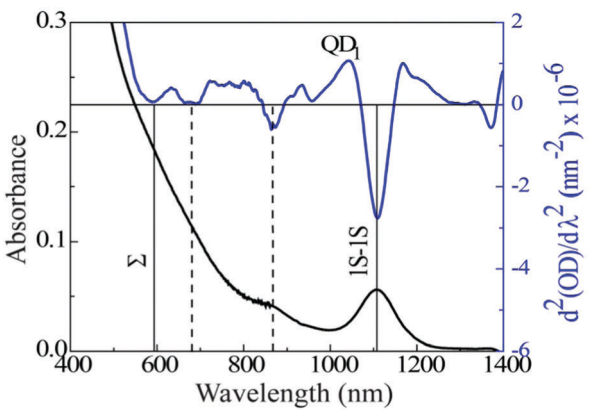

Fig. 2 QD_1 absorption spectra (black line) and their second derivative (blue line).

To identify the optical transitions of the three QDs, the second derivatives of their absorption spectra were calculated and are reported in Fig. 2 for QD_1 and in Fig. S3 in the ESI† for QD_2 and QD_3.[28,38,39] The first minima of the second derivative curve in Fig. 2 around 600 nm has been unambiguously assigned to the Σ transition,[28,33] which can be detected by the visible TA measurements as shown and discussed in Section 3.3. The assignment of the second dip (~870 nm) is still under debate. Hui *et al.* assigned it, on the basis of theoretical calculations using a $k{\cdot}p$ model,[40–42] to the $1S_{he}1P_{eh}$ transition, that is not optically allowed.§ Liljeorth *et al.* and several others defined this second transition as $1P_{he}1P_{eh}$ based on pump–probe measurements and density of states measured by scanning tunnelling spectroscopy.[43–46] The last minima of the second derivative curve at ~1100 nm which corresponds to the first excitonic absorption peak is assigned to the 1S–1S transition.[28]

3.2 Near infrared transient absorption (NIR TA) spectra and MEG QY

Fig. 3(a)–(c) show the NIR TA spectra of QD_1 at pump wavelengths of 800 nm (corresponding to $1.38E_g$), 400 nm ($2.75E_g$) and 267 nm ($4.14E_g$). The results for QD_2 and QD_3 can be found in Fig. S4 and S5 in the ESI,† respectively. For all the pump wavelengths the laser fluence was kept low enough to reduce the multiphoton absorption by QDs. Pump fluences of 10 μJ cm^{-2} (4.03×10^{13} photons per pulse per cm^2) for 800 nm and 5 μJ cm^{-2} (1.01×10^{13} photons per pulse per cm^2 for 400 nm and 0.67×10^{13} photons per pulse per cm^2 for 267 nm) for 400 nm and 267 nm pump wavelengths were used in TA measurements. The average number of photons absorbed per pulse by a QD, N_{abs}, was calculated using the product of the fluence (f) and the absorption cross-section (σ) at the pump wavelength ($N_{abs} = f{\cdot}\sigma$).[47] The absorption cross-sections were calculated following the method proposed by Giblin *et al.*[48] All the details of the method are reported in the ESI.† N_{abs} values at pump wavelengths of 800 nm, 400 nm and 267 nm are 0.031, 0.042 and 0.172 for QD_1, 0.037, 0.050 and 0.203 for QD_2 and 0.054, 0.072 and 0.294 for QD_3, respectively. The fluence dependent kinetics of QD_1 at 800 nm pump and 1100 nm probe wavelengths is reported in Fig. S6, in the ESI† showing that all the measurements were performed in a low fluency regime.

The spectra in Fig. 3(a)–(c) display similar features; however the time evolution for three pump wavelengths is different. The positive band around 1000 nm is due to the excited state absorption (ESA).[40,41] The main negative signal dominating the spectra at around 1100 nm corresponds to the ground state photobleaching (GSB). The GSB is due to depletion of the ground state carriers to excited states and it represents the 1S–1S

§ The $k{\cdot}p$ model is usually used to calculate the band structure and optical properties of crystalline materials. In the $k{\cdot}p$ model, the analysis of the perturbed term $k{\cdot}p$ (where k is the wave vector and p is the momentum operator vector) of the Hamiltonian provide information of the energy levels and the wave function of the energy levels.

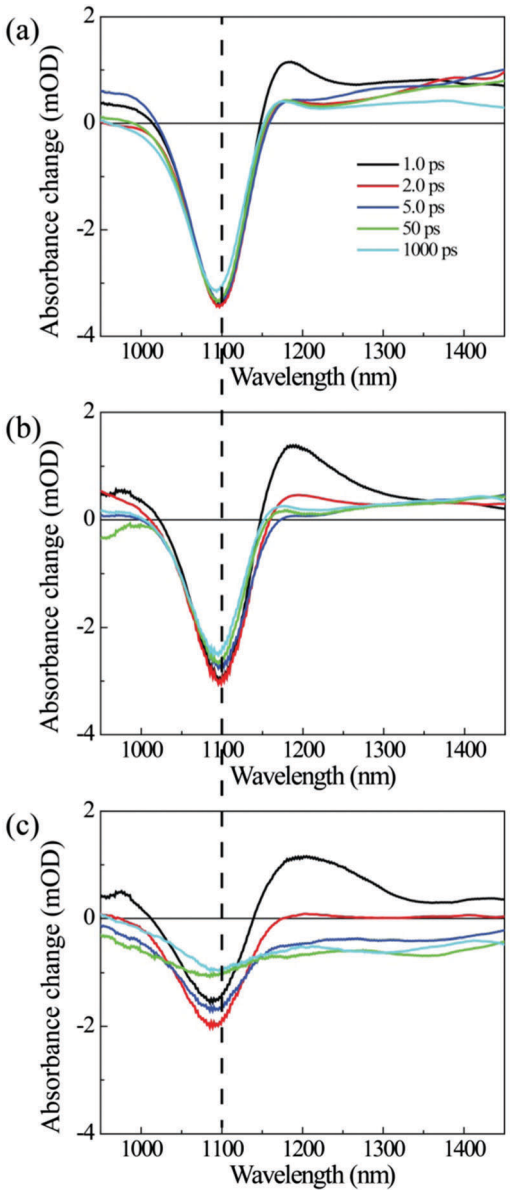

Fig. 3 TA spectra of PbSe QD_1 at pump wavelengths of (a) 800 nm, (b) 400 nm and (c) 267 nm.

transition as discussed before.[21,28,49,50] In addition to the GSB valley, a broad positive band at longer wavelengths due to the Coulomb interaction between the excitons is observed.[21]

In Fig. 4, the GSB dynamics of QD_1 at different pump wavelengths are shown after normalization with their long time tail. After excitation at 800 nm ($1.38E_g$, black circle), the kinetics shows a fast increase (<0.5 ps), a small and fast decaying differential signal in the first few ps due to a small amount of multi-photon absorption followed by a very long decay, much longer than our time scale of 1 ns. The long decay has been attributed to single exciton radiative recombination, which is of the order of microseconds in PbSe QDs.[26,32] The kinetics at 400 nm pump wavelength ($2.75E_g$, blue squares) shows a fast increase and then a fast decay in first tens of ps and followed by a long decay. The fast decay could be due to the Auger recombination

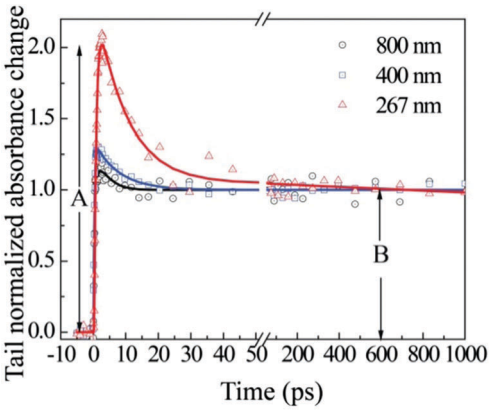

Fig. 4 QD_1 tail normalized TA kinetics at pump wavelengths of 800 (black circle), 400 (blue square) and 267 nm (red triangle) and a probe wavelength of 1100 nm. Symbols are data points and solid lines are bi-exponential fits.

of multiple hot excitons in QDs before relaxing into the long lived single exciton state.[26] For 267 nm excitation ($4.14E_g$, red triangles), we observe a slow increase around 1 ps and a fast decay in the first 50 ps followed by a long decay. The slow rise time can be explained as the cooling down process of hot excitons towards the band edge and the fast decay is due to a more efficient Auger recombination of multiple excitons with higher energy excitation. It is also reflected as a blue shift of the GSB signal (~10 nm at 1 ps delay) in Fig. 3(c).[21] The observation of Auger recombination of hot excitons and their lifetimes in PbSe QDs coincide well with previous literature results.[26,32]

From these decays it is possible to evaluate the MEG process and its quantum yield. MEG QY is defined as the number of excitons generated per photon absorbed. Experimentally, MEG QY can be calculated as A/B from the dynamics of the exciton GSB signal at the bandgap.[2,51] Indeed, assuming A is the maximum amplitude value of the dynamics, which is around 1 ps in our cases, and B is the amplitude of dynamics at long delay time, as shown in Fig. 4, MEG QY can be calculated as A/B for all the dynamics:[2,51]

$$\text{MEG QY} = A/B \quad (1)$$

Direct generation of multiple excitons *via* absorption of multiple photons can be misleading to measure MEG QY.[52,53] For determining the accuracy of MEG estimation, we have taken into account the influence of direct generation of multiple excitons *via* absorption of multiple photons introducing a correction factor in eqn (1) based on a Poisson distribution of photon absorption [$p = (1 - \exp(-N_{abs}))/N_{abs}$].[21] Accurate MEG QY can be calculated using the following equation:

$$\text{MEG QY} = p(A/B) \quad (2)$$

In our measurements we have evaluated MEG QY = 1.11 close to the theoretical MEG QY = 1 value at 800 nm ($1.38E_g$) excitation. At 400 nm ($2.75E_g$) excitation MEG QY was 1.25, which implies that multiple excitons were likely generated by one photon since the excitation photon energy is more than two times the bandgap energy ($2.75E_g$). On the other hand, MEG QY = 1.84,

Table 1 Pump wavelengths, corresponding $h\nu/E_g$ values and MEG QYs for QD_1, QD_2 and QD_3

Pump wavelength (nm)	QD_1		QD_2		QD_3	
	$h\nu/E_g$	MEG QY	$h\nu/E_g$	MEG QY	$h\nu/E_g$	MEG QY
800	1.38	1.11	1.50	1.13	1.63	1.13
400	2.75	1.25	3.00	1.28	3.25	1.33
267	4.12	1.84	4.49	2.07	4.87	2.17

meaning that approximately two excitons were generated per absorbed photon at 267 nm ($4.14E_g$) excitation. The MEG QYs of QD_2 and QD_3 were also determined at the same excitation wavelength and the corresponding TA dynamics are shown in Fig. S7(a) and (b) (ESI†), respectively.

Table 1 summarizes the calculated MEG QY for QD_1, QD_2 and QD_3. MEG QY varies for different sizes of QDs as a function of the excitation photon energy and bandgap energy ratio ($h\nu/E_g$). the MEG QY *versus* $h\nu/E_g$ plot is shown in the ESI,† Fig. S8. From a linear fit, the extracted MEG QYs at $4E_g$ for QD_1, QD_2 and QD_3 are 1.82, 1.77 and 1.70, respectively.[54] Here, we conclude that the photon energy at 400 nm is close to the threshold energy for the MEG process to overcome the phonon relaxation. Our results are consistent with the threshold values of $2.5E_g$–$3.0E_g$ reported for similar sizes of PbSe QDs.[35,55]

3.3 Visible transient absorption (TA) spectra

The visible TA spectra of PbSe QD_1, QD_2 and QD_3 in the range from 480 nm to 720 nm were measured for different pump wavelengths, below (800 nm), above (267 nm) and close (400 nm) to the MEG threshold, and are presented in the ESI,† Fig. S8–S10 in the time interval from 0 to 1000 ps.

The TA spectra at 5 and 100 ps pump–probe delays at 800 nm excitation (where no MEG process occurs) are shown in Fig. 5(a)–(c) for QD_1, QD_2 and QD_3, respectively together with their first derivative absorption spectra The TA spectra show a photo-induced absorption signal (positive) over the entire visible range. In a previous work, the photo-induced absorption peak for PbSe QDs has been attributed to the Coulomb interaction between the excitons generated by the pump and the excitons generated by the probe pulse.[56] In the same paper, it has been shown that the TA spectra divided by the first derivative of the linear absorption spectrum are proportional to the intensity of the Coulomb interaction energy, J. Moreover, the authors found that the Coulomb interaction is nearly wavelength independent above 550 nm and that the transient signal close to the band edge photo-bleaching signal has a rise time followed by a slow dynamics corresponding to the band-edge exciton radiative lifetime. The first implies that Coulomb interaction J is independent of the energy level of the probe exciton. The second implies that the Coulomb interaction of the newly created exciton hot pump exciton with the hot probe exciton, J_{HH}, is much smaller than the interaction after the thermal relaxation of the hot pump exciton to the band edge (cold) J_{HC}, $|J_{HH}| \ll |J_{HC}|$. Our data above 550 nm well reproduce the previous observations. In addition, we also present data in the spectral range smaller than 550 nm showing that J decreases

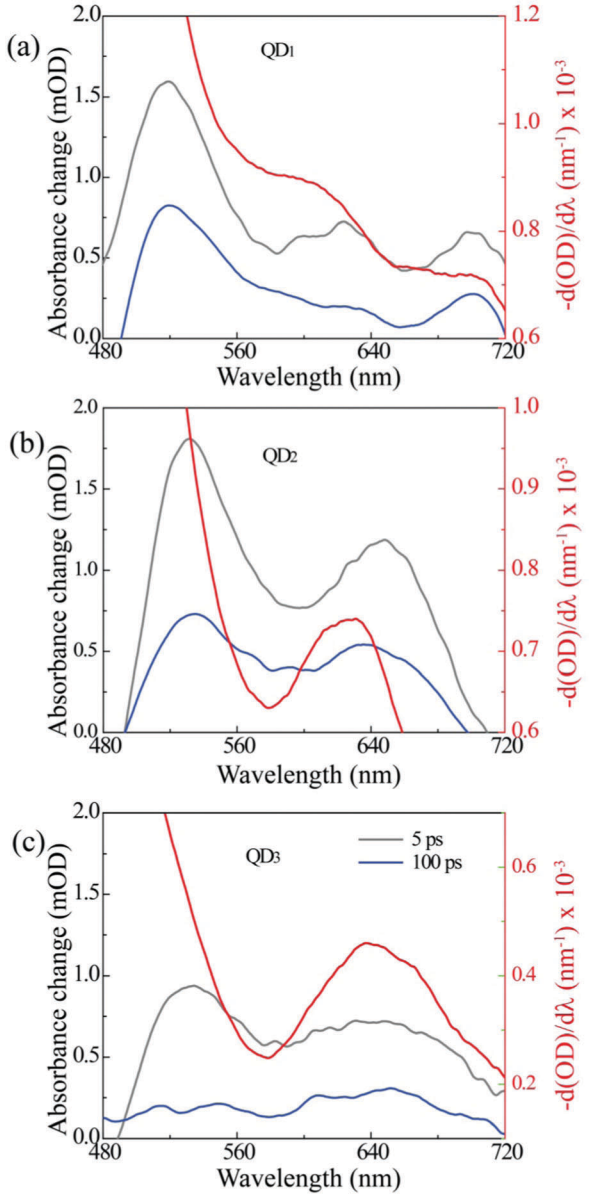

Fig. 5 TA spectra at 5 ps (gray line) and 100 ps (blue line) delays with the first derivative of absorption spectra (red line) of (a) QD_1, (b) QD_2 and (c) QD_3 using 800 nm pump wavelength.

rapidly below 530 nm and vanishes at 480 nm, implying that Coulomb interaction is not effective at highly excited energy levels. A fast dynamics for the peak centred ~525 nm is due to a thermalization process within the fine energy levels far from the band edge. The thermalization does not affect the photo-bleaching of the 1100 nm probe (black circles in Fig. 4) because the population of the band edge energy level does not change, but it can affect the Coulomb interaction with higher energy states.

In order to study the single exciton relaxation below, close to and above the MEG threshold energy, we analyse the TA spectra (Fig. 6) and dynamics (Fig. 7(a)–(c)) of QD_1at pump energies of 800 nm, 400 nm and 267 nm. We focus our discussion here on

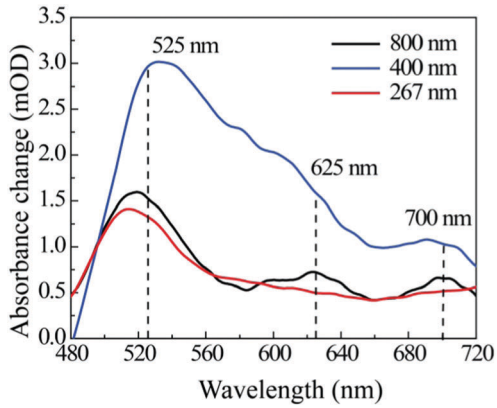

Fig. 6 TA spectra (at 5 ps delay) of QD_1 using pump wavelengths of 800 nm (below MEG threshold energy, black line), 400 nm (close to MEG threshold energy, blue line) and 267 nm (above MEG threshold energy, red line).

QD_1 since we found similar trends for all QDs. Both the spectra and TA dynamics of QD_1, QD_2 and QD_3 are provided in the ESI,† (Fig. S9 to S13). In Fig. 6, the TA spectra of QD_1 at 5 ps delay at the three pump energies are reported, the spectra are qualitatively similar at all delay times. The TA spectra at three pump wavelengths show peaks at 525 nm, 625 nm and 700 nm. The spectrum at a pump wavelength of 400 nm (close to the MEG threshold) exhibits a strong and structured photo-induced signal at 625 nm and 525 nm, while the spectra at 800 nm and 267 nm wavelengths are very similar showing a less structured signal. Geiregat *et al.* studied the TA spectra of PbSe QDs in the visible region.[4] When they used pump energy above the Σ transition they observed a fast photo-bleaching (a fast negative signal in the first 1–2 ps) for probe energy corresponding to the Σ point. Conversely, when using pump energy below the Σ transition, they did not observe any bleaching. In our measured visible TA spectra of PbSe QDs, we do not observe any bleaching both at pumping energies above and below the Σ transition (Fig. S9–S11, ESI†) maybe due to the weak bleaching signal, and thus it could be hidden by the noise.

Fig. 7 shows the normalized dynamics of the hot excitons, TA signal generated at 800 nm (a), 400 nm (b) and 267 nm (c) excitation and probe wavelengths of 525 nm, 625 nm and 700 nm. The TA dynamics were deconvoluted and fitted by a single exponential rise and decay plus a constant for the long decays. In Fig. 7(a) where no MEG process occurs, the fast rise/decay times are about 0.2 ps/2 ps at 525 nm, 0.3 ps/3 ps at 625 nm and 0.5 ps/4 ps at 700 nm. After very fast decay, the curves reach an almost asymptotic value at all wavelengths, as illustrated in the inset of Fig. 7(a). This very long decay time is associated with the radiative recombination of the excitons at the band edge.[56]

The TA dynamics of QD_1 excited at 400 nm are shown in Fig. 7(b); a remarkable difference from the decay obtained at 800 nm excitation was observed. Indeed, the rise times at 525 nm are similar at both pump excitation wavelengths (0.2 ps at 800 nm, 0.1 ps at 400 nm), while the rise times at 625 nm (1 ps) and 700 nm (2 ps) are longer at 400 nm pump wavelength. A similar behaviour is observed for QD_2 and QD_3 (Fig. S12 and S13 in ESI†).

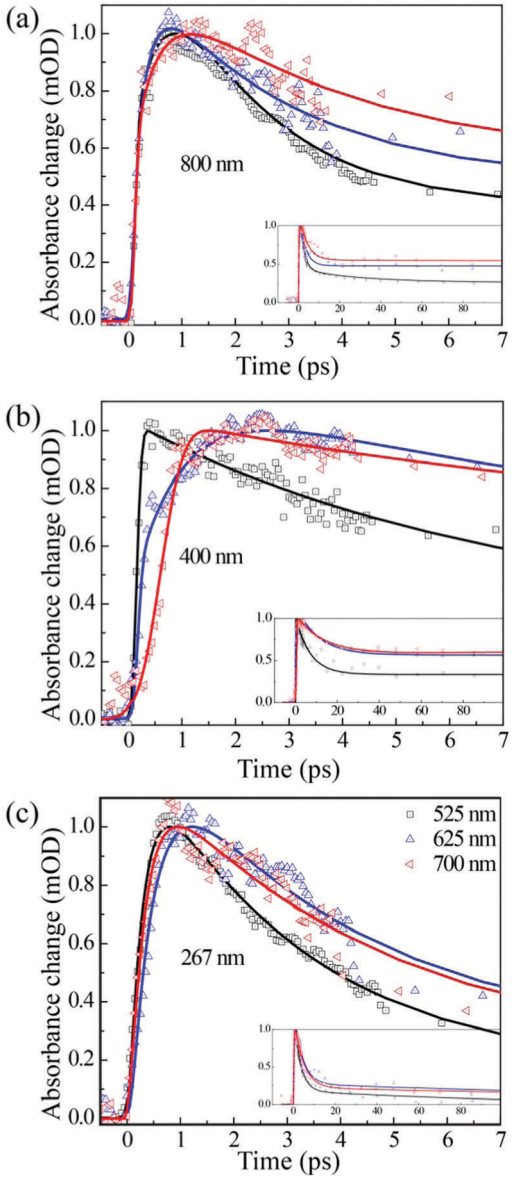

Fig. 7 Normalized TA dynamics of QD_1 using pump wavelengths of (a) 800 nm, (b) 400 nm and (c) 267 nm. In each figure, probe wavelengths are 525 nm (black), 625 nm (blue) and 700 nm (red). The insets of figures show kinetics for long delays. Symbols are data points and solid lines are bi-exponential fits.

Moreover, TA dynamics present rather long decay times (around 5 ps at 525 nm, 10 ps at 625 nm and 13 ps at 700 nm probe wavelength) as compared to those observed in the 800 nm and 267 nm pump cases, as will be discussed later. We recall that the Σ transition lays around 600 nm, *i.e.* in between the 525 nm and the 625 nm peaks, as illustrated in Fig. 2 and in Fig. S3 (ESI†). Given that the Σ transition is around 600 nm for PbSe QDs, the hot excitons generated by the 400 nm pump thermally relaxes towards the Σ level, and thus, the fast rise of photo-induced absorption signal probed at 525 nm can be related to the quick thermal relaxation of hot excitons towards the Σ level. Around the Σ transition, there is a bottleneck for the phonons, which

slows down the thermal relaxation of hot excitons. Therefore, the hot exciton dynamics probed above 600 nm (625 nm and 700 nm) present a much slower rise and a longer decay time. The long decay after 30 ps reflects the exciton radiative lifetime. There is still an on-going debate regarding the existence of the phonon bottleneck.[57,58] Some previous studies have attributed the slowing down of charge carrier cooling to the a phonon scattering bottleneck in a critical point of the Brillouin zone,[4,58] while others do not support this interpretation since the high energy levels are continuous.[57] Prezhdo *et al.* suggested the presence of the electron–phonon bottleneck in the semi-discrete energy levels just above the bandgap.[57] Our results seem to support the existence of the electron–phonon bottleneck around the Σ transition.

The TA dynamics of QD_1 pumped by the 267 nm beam shows a trend similar to that of the 800 nm pump (Fig. 7(c)) with a slightly longer rise time (about 1 ps) corresponding to the MEG cooling.[19] The fast decay times are around 3.5 ps, 4 ps and 4.5 ps for 525 nm, 625 nm and 700 nm probe wavelengths, respectively. The analogy of 800 nm and 267 nm pump dynamics implies that the hot exciton relaxes following the same process once generated regardless of whether the MEG occurred in QD_1. On the other hand, around the MEG threshold energy (Fig. 7(b)), the phonon bottleneck due to the Σ transitions becomes significant so the hot exciton cooling process has to overtake the phonon relaxation channel in order to overcome the MEG threshold. It is clear that when pump energy is well above the threshold, MEG dominates over phonon relaxation: the highly energetic exciton generated by the 267 nm pump photon quickly decays to the band edge, by creating additional excitons; the additional excitons recombine non-radiatively *via* Auger recombination by giving up their energy to the third charge; finally, the last exciton decays radiatively.

Geiregat *et al.* calculated the coulomb interaction energy of excitons and found it to be proportional to the number of excitons. So, the amplitude of the TA spectra should also be proportional to the number of generated excitons. In a similar way, we suggest that it is possible to estimate the MEG QY by comparing the dynamics in the visible region following the same definition of MEG QY at the bandgap instead of calculating the Coulomb interaction energy of excitons. In other words, the ratio between the values of A and B for the kinetics in the visible region at different excitation wavelengths can be an estimation of the MEG QY. Indeed, the A/B ratio has been measured at 525 nm probe wavelength ($(A/B)_{525}$) and at excitation wavelengths of 800 nm, 400 nm and 267 nm for QD_1, QD_2, and QD_3 as shown in Fig. S14 and Table S1 (ESI†). As discussed before, just after the excitation, hot–hot, hot–cold and cold–cold exciton interactions, *etc.* take place. Due to these effects, the $(A/B)_{525}$ values can be higher than the A/B values. Since there is no MEG at 800 nm excitation, the $(A/B)_{525}$ values at all three excitation wavelengths are normalized with respect to the $(A/B)_{525}$ value obtained at 800 nm, the results are shown in Table 2. MEG QY_{525} is comparable to the MEG QY for all three measured QDs as shown in Table 1. Therefore, here we demonstrate that MEG QY can be measured in the visible region above the band gap of QDs. This observation deserves further investigation.

Table 2 MEG QY_{525} of PbSe QD_1, QD_2 and QD_3 at 525 nm probe wavelength and 800 nm, 400 nm and 267 nm pump wavelengths

	MEG QY_{525}		
Pump wavelength (nm)	QD_1	QD_2	QD_2
800	1	1	1
400	1.10	1.16	1.09
267	2.19	2.29	2.38

4. Conclusions

In this work, we study the TA spectra of PbSe QDs of three sizes ranging from 3.6 nm to 4.3 nm and their dynamics in NIR and visible regions. MEG QYs were measured at the band gap at different excitation photon energies and the values extrapolated at four times the QD band gap are 1.82, 1.77 and 1.70 for QD_1, QD_2 and QD_3, respectively.

The visible TA spectra were studied around the Σ transition at different pump energies: below, close to and above the MEG threshold. Our analysis provides clear evidence of the role of the Σ transition in slowing down the exciton cooling process. The universality of this behaviour is confirmed by a similar behaviour displayed by QDs of different sizes. In conclusion, here we show that TA spectra dynamics in the visible range can provide essential information to interpret the dynamics of MEG and possibly use it to assess the MEG QY.

Acknowledgements

The authors wish to thank the Singapore Ministry of Education for financial support through projects MOE2013-T2-1-044 and MOE2011-T3-1-005.

Notes and references

1 M. C. Hanna and A. J. Nozik, *J. Appl. Phys.*, 2006, **100**, 074510.
2 R. D. Schaller and V. I. Klimov, *Phys. Rev. Lett.*, 2004, **92**, 186601.
3 A. Le Bris and J.-F. Guillemoles, *Appl. Phys. Lett.*, 2010, **97**, 113506.
4 P. Geiregat, C. Delerue, Y. Justo, M. Aerts, F. Spoor, D. van Thourhout, L. D. A. Siebbeles, G. Allan, A. J. Houtepen and Z. Hens, *ACS Nano*, 2015, **9**, 778.
5 M. C. Beard, A. G. Midgett, M. C. Hanna, J. M. Luther, B. K. Hughes and A. J. Nozik, *Nano Lett.*, 2010, **10**, 3019.
6 O. E. Semonin, J. M. Luther, S. Choi, H.-Y. Chen, J. Gao, A. J. Nozik and M. C. Beard, *Science*, 2011, **334**, 1530.
7 L. A. Padilha, J. T. Stewart, R. L. Sandberg, W. K. Bae, W.-K. Koh, J. M. Pietryga and V. I. Klimov, *Nano Lett.*, 2013, **13**, 1092.
8 A. G. Midgett, J. M. Luther, J. T. Stewart, D. K. Smith, L. A. Padilha, V. I. Klimov, A. J. Nozik and M. C. Beard, *Nano Lett.*, 2013, **13**, 3078.

9 P. D. Cunningham, J. E. Boercker, E. E. Foos, M. P. Lumb, A. R. Smith, J. G. Tischler and J. S. Melinger, *Nano Lett.*, 2011, **11**, 3476.
10 J. J. H. Pijpers, R. Ulbricht, K. J. Tielrooij, A. Osherov, Y. Golan, C. Delerue, G. Allan and M. Bonn, *Nat. Phys.*, 2009, **5**, 811.
11 Q. Shen, K. Katayama and T. Toyoda, *J. Energy Chem.*, 2015, **24**, 712.
12 J. Gao, A. F. Fidler and V. I. Klimov, *Nat. Commun.*, 2015, **6**, 8185.
13 S. Ten Cate, C. S. S. Sandeep, Y. Liu, M. Law, S. Kinge, A. J. Houtepen, J. M. Schins and L. D. A. Siebbeles, *Acc. Chem. Res.*, 2015, **48**, 174.
14 A. Al-Otaify, S. V. Kershaw, S. Gupta, A. L. Rogach, G. Allan, C. Delerue and D. J. Binks, *Phys. Chem. Chem. Phys.*, 2013, **15**, 16864.
15 A. Sills and M. Califano, *Phys. Chem. Chem. Phys.*, 2015, **17**, 2573.
16 Z. E. R. Abrams, M. Gharghi, A. Niv, C. Gladden and X. Zhang, *Sol. Energy Mater. Sol. Cells*, 2012, **99**, 308.
17 N. J. L. K. Davis, M. L. Bohm, M. Tabachnyk, F. Wisnivesky-Rocca-Rivarola, T. C. Jellicoe, C. Ducati, B. Ehrler and N. C. Greenham, *Nat. Commun.*, 2015, **6**, 8259.
18 M. L. Böhm, T. C. Jellicoe, M. Tabachnyk, N. J. L. K. Davis, F. Wisnivesky-Rocca-Rivarola, C. Ducati, B. Ehrler, A. A. Bakulin and N. C. Greenham, *Nano Lett.*, 2015, **15**, 7987.
19 R. J. Ellingson, M. C. Beard, J. C. Johnson, P. Yu, O. I. Micic, A. J. Nozik, A. Shabaev and A. L. Efros, *Nano Lett.*, 2005, **5**, 865.
20 M. C. Beard, K. P. Knutsen, P. Yu, J. M. Luther, Q. Song, W. K. Metzger, R. J. Ellingson and A. J. Nozik, *Nano Lett.*, 2007, **7**, 2506.
21 J. Sun, W. Yu, A. Usman, T. T. Isimjan, S. Dgobbo, E. Alarousu, K. Takanabe and O. F. Mohammed, *J. Phys. Chem. Lett.*, 2014, **5**, 659.
22 A. A. O. El-Ballouli, E. Alarousu, A. Usman, J. Pan, O. M. Bakr and O. F. Mohammed, *ACS Photonics*, 2014, **1**, 285.
23 D. J. Binks, *Phys. Chem. Chem. Phys.*, 2011, **13**, 12693.
24 I. Gdor, C. Yang, D. Yanover, H. Sachs, E. Lifshitz and S. Ruhman, *J. Phys. Chem. C*, 2013, **117**, 26342.
25 G. Nair, S. M. Geyer, L.-Y. Chang and M. G. Bawendi, *Phys. Rev. B: Condens. Matter Mater. Phys.*, 2008, **78**, 125325.
26 J. A. McGuire, M. Sykora, J. Joo, J. M. Pietryga and V. I. Klimov, *Nano Lett.*, 2010, **10**, 2049.
27 S. J. O. Hardman, D. M. Graham, S. K. Stubbs, B. F. Spencer, E. A. Seddon, H.-T. Fung, S. Gardonio, F. Sirotti, M. G. Silly, J. Akhtar, P. O'Brien, D. J. Binks and W. R. Flavell, *Phys. Chem. Chem. Phys.*, 2011, **13**, 20275.
28 R. Koole, G. Allan, C. Delerue, A. Meijerink, D. Vanmaekelbergh and A. J. Houtepen, *Small*, 2008, **4**, 127.
29 G. Nootz, L. A. Padilha, L. Levina, V. Sukhovatkin, S. Webster, L. Brzozowski, E. H. Sargent, D. J. Hagan and E. W. Van Stryland, *Phys. Rev. B: Condens. Matter Mater. Phys.*, 2011, **83**, 155302.
30 A. Lipovskii, E. Kolobkova, V. Petrikov, I. Kang, A. Olkhovets, T. Krauss, M. Thomas, J. Silcox, F. Wise, Q. Shen and S. Kycia, *Appl. Phys. Lett.*, 1997, **71**, 3406.
31 J. M. Pietryga, D. J. Werder, D. J. Williams, J. L. Casson, R. D. Schaller, V. I. Klimov and J. A. Hollingsworth, *J. Am. Chem. Soc.*, 2008, **130**, 4879.
32 R. D. Schaller, V. M. Agranovich and V. I. Klimov, *Nat. Phys.*, 2005, **1**, 189.
33 J. E. Murphy, M. C. Beard, A. G. Norman, S. P. Ahrenkiel, J. C. Johnson, P. Yu, O. I. Mićić, R. J. Ellingson and A. J. Nozik, *J. Am. Chem. Soc.*, 2006, **128**, 3241.
34 J. A. McGuire, J. Joo, J. M. Pietryga, R. D. Schaller and V. I. Klimov, *Acc. Chem. Res.*, 2008, **41**, 1810.
35 C. Smith and D. Binks, *Nanomaterials*, 2013, **4**, 19.
36 T. Nishihara, H. Tahara, M. Okano, M. Ono and Y. Kanemitsu, *J. Phys. Chem. Lett.*, 2015, **6**, 1327.
37 M. Bradler, P. Baum and E. Riedle, *Appl. Phys. B: Lasers Opt.*, 2009, **97**, 561.
38 S. L. Sewall, R. R. Cooney, K. E. H. Anderson, E. A. Dias and P. Kambhampati, *Phys. Rev. B: Condens. Matter Mater. Phys.*, 2006, **74**, 235328.
39 L. Cademartiri, E. Montanari, G. Calestani, A. Migliori, A. Guagliardi and G. A. Ozin, *J. Am. Chem. Soc.*, 2006, **128**, 10337.
40 J. J. Peterson, L. Huang, C. Delerue, G. Allan and T. D. Krauss, *Nano Lett.*, 2007, **7**, 3827.
41 J. M. Harbold, H. Du, T. D. Krauss, K.-S. Cho, C. B. Murray and F. W. Wise, *Phys. Rev. B: Condens. Matter Mater. Phys.*, 2005, **72**, 195312.
42 H. Du, C. Chen, R. Krishnan, T. D. Krauss, J. M. Harbold, F. W. Wise, M. G. Thomas and J. Silcox, *Nano Lett.*, 2002, **2**, 1321.
43 P. Liljeroth, P. A. Z. van Emmichoven, S. G. Hickey, H. Weller, B. Grandidier, G. Allan and D. Vanmaekelbergh, *Phys. Rev. Lett.*, 2005, **95**, 086801.
44 J. M. Schins, M. T. Trinh, A. J. Houtepen and L. D. A. Siebbeles, *Phys. Rev. B: Condens. Matter Mater. Phys.*, 2009, **80**, 035323.
45 M. T. Trinh, A. J. Houtepen, J. M. Schins, J. Piris and L. D. A. Siebbeles, *Nano Lett.*, 2008, **8**, 2112.
46 I. Gdor, H. Sachs, A. Roitblat, D. B. Strasfeld, M. G. Bawendi and S. Ruhman, *ACS Nano*, 2012, **6**, 3269.
47 J. M. Luther, M. C. Beard, Q. Song, M. Law, R. J. Ellingson and A. J. Nozik, *Nano Lett.*, 2007, **7**, 1779.
48 J. Giblin and M. Kuno, *J. Phys. Chem. Lett.*, 2010, **1**, 3340.
49 P. Kambhampati, *J. Phys. Chem. C*, 2011, **115**, 22089.
50 K. Zheng, K. Žídek, M. Abdellah, W. Zhang, P. Chábera, N. Lenngren, A. Yartsev and T. Pullerits, *J. Phys. Chem. C*, 2014, **118**, 18462.
51 M. Ji, S. Park, S. T. Connor, T. Mokari, Y. Cui and K. J. Gaffney, *Nano Lett.*, 2009, **9**, 1217.
52 K. J. Karki, F. Ma, K. Zheng, K. Zidek, A. Mousa, M. A. Abdellah, M. E. Messing, L. R. Wallenberg, A. Yartsev and T. Pullerits, *Sci. Rep.*, 2013, **3**, 2287.
53 N. Lenngren, T. Garting, K. Zheng, M. Abdellah, N. Lascoux, F. Ma, A. Yartsev, K. Žídek and T. Pullerits, *J. Phys. Chem. Lett.*, 2013, **4**, 3330.
54 M. Aerts, T. Bielewicz, C. Klinke, F. C. Grozema, A. J. Houtepen, J. M. Schins and L. D. A. Siebbeles, *Nat. Commun.*, 2014, **5**, 3789.
55 S. ten Cate, Y. Liu, C. S. Suchand Sandeep, S. Kinge, A. J. Houtepen, T. J. Savenije, J. M. Schins, M. Law and L. D. A. Siebbeles, *J. Phys. Chem. Lett.*, 2013, **4**, 1766.
56 P. Geiregat, A. Houtepen, Y. Justo, F. C. Grozema, D. Van Thourhout and Z. Hens, *J. Phys. Chem. C*, 2014, **118**, 22284.
57 O. V. Prezhdo, *Chem. Phys. Lett.*, 2008, **460**, 1.
58 P. Yu, J. M. Nedeljkovic, P. A. Ahrenkiel, R. J. Ellingson and A. J. Nozik, *Nano Lett.*, 2004, **4**, 1089.

